# Predicting Response to Benzamide Riboside Chemotherapy in Hepatocellular Carcinoma Using Apparent Diffusion Coefficient of Water

ANDRIY M. BABSKY[1], SHENGHONG JU[1†], BEENA GEORGE[1], STACY BENNETT[1§], MINGSHENG HUANG[1‡], HIREMAGALUR N. JAYARAM[2,3], GORDON MCLENNAN[1§] and NAVIN BANSAL[1]

*Department of [1]Radiology and Imaging Sciences, and*
*[2]Biochemistry and Molecular Biology, Indiana School of Medicine, Indianapolis, IN, U.S.A.;*
*[3]Richard L. Roudebush Veterans Affairs Medical Center, Indianapolis, IN, U.S.A.*

**Abstract.** *Aim: To monitor the effects of the apoptotic agent benzamide riboside (BR) on tumor volume and water apparent diffusion coefficient (ADC) in rat hepatocellular carcinoma (HCC). Materials and Methods: Water ADC of the tumors and nearby liver tissue was measured using diffusion-weighted $^1$H MRI (DWI). The two groups of BR-treated animals, which differed in their sensitivity to the treatment, were identified as responsive ($R_{BR}$) and non-responsive ($NR_{BR}$). Results: Tumor growth in the $R_{BR}$ group was arrested and the mean tumor volume in this group was 1/6th and 1/16th compared to that of the $NR_{BR}$ group on days 7 and 14 after treatment, respectively. Water ADC of HCC was higher than in nearby normal liver tissue. Before BR treatment, the mean water ADC was significantly higher in the $R_{BR}$ group compared to the $NR_{BR}$ group. BR therapy did not change the water ADC value regardless of tumor sensitivity. Conclusion: Although the water ADC did not change after chemotherapy by BR, DWI has great potential for detecting and predicting response to chemotherapy in HCC.*



*Current address:* †Department of Radiology, Zhongda Hospital, Southeast University, Nanjing, P.R. China; §Imaging Institute, Cleveland Clinic, Cleveland, OH, U.S.A.; ‡Department of Interventional Radiology, Sun Yat-sen University, Guangzhou, P.R. China

*Correspondence to:* Andriy Babsky, Ph.D., D.Sc., Department of Radiology and Imaging Sciences, Indiana University School of Medicine, 950 West Walnut Street, R2 E124, Indianapolis, IN 46202-5181, U.S.A. Tel: +1 3172789681, Fax: +1 3172741067, e-mail: ababsky@iupui.edu

*Key Words:* Hepatocellular carcinoma, $^1$H MRI, apparent diffusion coefficient, extracellular space, benzamide riboside, angiography, therapy response, motion effect.

Hepatocellular carcinoma (HCC) and liver metastases from colon and breast carcinomas are an increasing problem worldwide, representing the third largest cause of cancer-related death (1). It is becoming a great health problem not only in Asia and Africa, but also in Western countries mostly due to the major risk factors of HCC growth, such as cirrhosis and hepatitis, which encourage genetic changes that lead to neoplastic transformations (1). As many chemotherapy regimens have been developed for HCC treatment, accurate, non-invasive and quantitative monitoring of the early response to chemotherapy is critical as this data may indicate a need for alteration in therapy. An accurate monitoring scheme would also result in a reduction of invasive needle biopsies.

Chemotherapy efficiency has been estimated in a number of animal studies by using water apparent diffusion coefficient (ADC) measured by diffusion-weighted $^1$H MRI (DWI) (2-3). However, measurement of water ADC in abdominal tumors is challenging due to its sensitivity to respiratory, cardiovascular and/or gastrointestinal motions (4). To avoid these difficulties, most studies on the effect of chemotherapy on water ADC in rodent tumor models have used tumors placed subcutaneously (5-7). In patients, DWI of tumors and liver is a common technique because of the ability to breath-hold combined with the recent technology of single-shot echo-planar imaging with fat suppression (8-9). However, in the rat HCC model, water ADC in tumor and surrounding liver tissue has been evaluated only in a few studies (10-11). Thus, estimation of water ADC in orthotopic HCC before and after treatment is essential.

Benzamide riboside (1-β-D-ribofuranosylbenzene-3-carboxamide, BR) is novel antitumor drug (12). In fact, BR is a nucleoside prodrug that is metabolized intracellularly in malignant cells to an analog of NAD, benzamide adenine dinucleotide, that strongly and selectively inhibits inosine-5'-monophosphate dehydrogenase, which is the rate-limiting step of *de novo* guanylate synthesis. This action interferes with nucleic acid metabolism by halting DNA and RNA synthesis (12). BR induces apoptosis in K562, HL-60, and ovarian

carcinoma cell lines by depleting GTP. The exact mechanism of this activity is under investigation, but may involve the observed property that benzamide adenine dinucleotide inhibits malate dehydrogenase, a mitochondrial enzyme involved in cellular respiration. Because BR is metabolized in normal hepatocytes by carboxylation to an inactive benzene carboxylic acid riboside, BR has selective toxicity in liver, tumors while preserving normal hepatocytes (12). In our study BR was administered through the hepatic artery. HCC tissue is highly vascular and the main blood transportation is switched from the portal vein to the hepatic artery (13). The main advantage of hepato-arterial intervention is the possibility of increasing drug concentration in certain liver tumor regions and decreasing systemic toxicity.

In this study, the effects of BR delivered through the hepatic artery on HCC tumor volume and water ADC in tumor and surrounding liver tissue were examined to answer the following questions: i) Are pretreatment values of water ADC useful for predicting response to therapy? ii) Is water ADC affected following therapy? iii) Are changes in HCC volume and water ADC correlated?

## Materials and Methods

*Tumor model*. All animal studies were approved by the Indiana University Institutional Animal Care and Use Committee. N1S1 cells (American Type Tissue Culture Collection, Bethesda, MD, USA), a rat Novikoff hepatoma cell line, was maintained as an exponentially growing suspension in Iscove modified Dulbecco's Medium (Sigma-Aldrich, St. Louis, MO, USA). To create the intrahepatic HCC, $1\times10^6$ N1S1 cells were inoculated in the left lateral liver lobe of the male Sprague-Dawley rats (Harlan, Indianapolis, IN, USA) weighing 450-500 g. The tumors were allowed to grow for one week before the first MRI experiment and for two weeks before angiography. Tumor growth was measured from $T_2$ $^1$H images with *b*-value=0 s/mm$^2$. After the 28-day MRI experiment, livers containing tumors were excised for histology (Figure 1A). Doubling time of tumor growth was calculated using exponential curve of tumor volume on days 7, 14, 21, and 28 after cell injection.

*Hepatic angiography and BR treatment*. A 3-cm incision was made in the right groin to expose the femoral artery. A 5-mm incision was made longitudinally in the femoral artery and an Excel 14 microcatheter (Boston Scientific, Natick, MA, USA) and guide wire (Guidant, Indianapolis, IN, USA) were carefully inserted into the vessel with cannulation forceps (model 500377). When the wire was in the femoral artery, the tip was advanced under fluoroscopic guidance into the thoracic aorta and the catheter was able to track into the abdominal aorta. The catheter and guide wire were then used to select the common hepatic artery, and a rotational angiogram was obtained with a KX0-100 digital subtraction Carm unit (Toshiba, Tokyo, Japan) with rotational digital subtraction at 15°/s rotation at 15 fps, 66 kV, 125 mA, and 43 ms exposures (Figure 1B). Total contrast agent injection during rotational digital subtraction angiography was 3 mL of Hypaquemeglumine 60% (Amersham, Princeton, NJ, USA). BR (20 mg/kg) was then infused into 10 rats into the hepatic artery extending into the liver. The catheter was removed and the femoral artery was ligated(14).

*MRI experiments*. All *in vivo* MRI images were acquired with a Varian 9.4 Tesla, 31-cm horizontal bore system (Varian, Paolo Alto, CA, USA). HCC was examined weekly for 4 weeks after N1S1 cell inoculation. Animals were anesthetized with 1-1.5% isoflurane delivered in medical air at 1-1.5 l/min using a rat nose mask connected to a gas anesthesia machine (Vetland, Louisville, KY, USA). Rat respiration was monitored with a respiration module (SA Instruments, Stony Brook, NY, USA) using a sensitive transducer located under the animal's abdominal area. The magnet was shimmed to less than 140 Hz line width at half height of the $^1$H water signal.

*$^1$H MRI*. Water ADC of the tumors and nearby liver tissue were measured with a birdcage volume coil (ID=63 mm, length=190 mm) tuned to 400 MHz. The liver area was placed in the middle of the coil. Multi-slice DWIs of the tumor were collected using a spin-echo sequence consisting of two diffusion gradient pulses of $\delta$=6 ms duration separated by a $\Delta$=11 ms period applied along all three axis. Interleaved DWI with four *b*-values (*b*=0, 256, 945 and 1679 s/mm$^2$), 1100 ms repetition time (TR), 21 ms echo time (TE), 256×128 data points over a 64×64 field of view (FOV), 16 slices, 0.5 mm slice thickness, 1.5 mm slice gap were collected. Respiratory gating was used to minimize the motion effect on water ADC. In addition, the animal respiration rate was brought to a relatively stable level (≤40 breaths/min) to minimize variation in TR by slightly adjusting the isoflurane anesthesia. Water ADC was monitored only during the end-expiration time. Total data collection time for a set of DWI was 15 min. $^1$H images and water ADC maps were reconstructed using the Image Browser software provided by Varian. The tumor volume and average water ADC were determined over a three-dimensional (3D) volume of interest for each temporal measurement.

$^1$H diffusion data were fit to the Stejskal-Tanner equation (15). The average ADCs in intrahepatic tumor and surrounding liver were calculated using a $3\times10^{-3}$ mm$^2$/s threshold to eliminate abnormal ADC values that were clearly higher than the diffusion coefficient of free water (16). In general, the threshold process decreased the ADC values by ~25-30% eliminating a signal artifact related to the motion effects. Water ADC in HCC was compared to water ADC in surrounding liver tissue, which also exhibited motion effects.

*Histology*. The intrahepatic tumors with the surrounding liver tissue were excised from the animal body, fixed in 10% formalin solution (Fisher Scientific, Pittsburgh, PA, USA), and then embedded in paraffin. The histological sections of the tumors were cut along the same plane as the MR images. Tissue sections were obtained at 5 μm thickness and stained with hematoxylin and eosin (H&E) to identify the viable, necrotic, and inflammation tumor regions (Figure 1C).

*Data analysis and statistics*. All statistical data are presented as the mean±standard error of mean (SEM) and represent the range across a cohort of animals (n=12 (control group), 5 (responsive ($R_{BR}$), and 5 non-responsive to BR ($NR_{BR}$) groups). Analysis of the data was performed by ANOVA with *post-hoc* comparisons among the experimental groups and time points using the least significant difference test (Statistica/v. 5.1 program). A *p*-value ≤0.05 was used to define statistical significance.

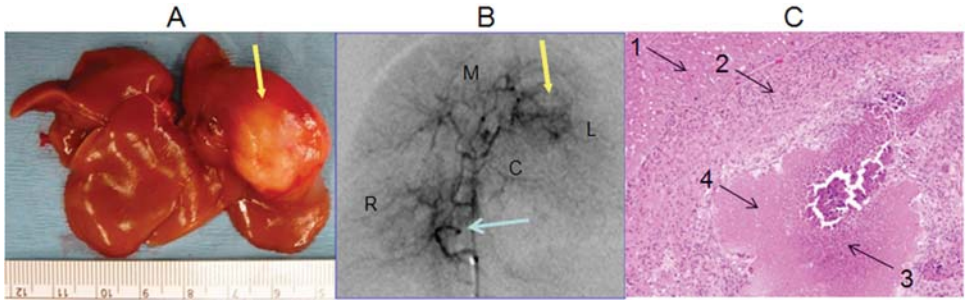


Figure 1. *A: Macroscopic appearance of HCC 28 days after N1S1 cell inoculation. Yellow arrow shows HCC location. B: Hepatic angiography via transfemoral approach. R, M, C, and L – Right, medium, central, and left lobes of the liver, respectively. Yellow arrow shows HCC location and blue arrow shows the tip of Excel-14 microcatheter. C: Hematoxylin/eosin-stained histological slice of the liver bearing HCC. 1 – Normal liver, 2 – viable HCC, 3 – inflammation, 4 – necrosis. Original magnification, ×200.*

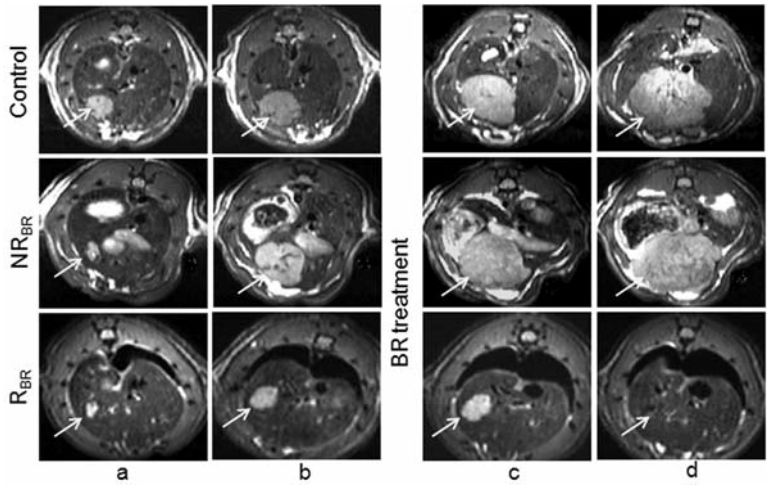


Figure 2. *Effect of transarterial treatment of HCC with BR. $T_2$-weighted MRI shows a tumor in the left lobe of the liver on days 7 (a), 14 (b), 21 (c), and 28 (d) after inoculation with $1\times10^6$ cells. In the $R_{BR}$ group, the tumor ceased to grow 7 days post BR intrahepatic artery treatment (20 mg/kg), and almost disappeared 14 days post treatment. Arrows indicate HCC.*

## Results

*Tumor volume*. The two groups of BR-treated animals, which differed in their sensitivity to the treatment as was estimated from tumor volume changes, were identified as $R_{BR}$ and $NR_{BR}$. Representative $T_2$ $^1$H MRI from control, $NR_{BR}$, and $R_{BR}$ groups are presented in Figure 2. In the $R_{BR}$ group, 7 days post BR treatment (20 mg/kg), the tumor ceased to grow, and almost disappeared on 14 days post treatment. In the $NR_{BR}$ group, the tumor continued to grow after BR treatment with a rate similar to that of the control group. The mean tumor volumes are shown in Figure 3A as calculated using $T_2$ weighted $^1$H MRI. The mean tumor volumes for all three groups were similar before treatment on day 7 (0.13±0.05 $cm^3$ for control group (A), 0.03±0.02 $cm^3$ for $NR_{BR}$ group (B), and 0.04±0.01 $cm^3$ for $R_{BR}$ group (C)). On day 14 the tumors grew to 0.85±0.19 $cm^3$ (control, $p\leq0.05$ *vs*. day 7), 0.40±0.16 $cm^3$ ($NR_{BR}$, $p\leq0.05$ *vs*. day 7), and 0.20±0.11 $cm^3$ ($R_{BR}$, $p\leq0.15$ *vs*. day 7). In the $NR_{BR}$ group, the tumors continued to grow during the next 1-and 2-week post-treatment to 1.51±0.71 $cm^3$ ($p\leq0.05$ *vs*. day 7) and 3.00±1.60 $cm^3$ ($p\leq0.07$ *vs*. day 7), respectively. Tumor growth in the $R_{BR}$ group was arrested: 0.24±0.12 $cm^3$ and 0.19±0.09 $cm^3$ in tumor volume on days 7 and 14 post-treatment, respectively. Furthermore, the mean tumor volume in the $R_{BR}$ group was 1/6th and 1/16th compared to the $NR_{BR}$ group ($p\leq0.05$) on days 7 and 14 after treatment, respectively. The doubling time of the tumor growth in control and $NR_{BR}$ groups was 3.2 and 3.9 days, respectively. In the control group, the tumors continued to grow during the third and fourth weeks of experiments to 2.58±0.52 $cm^3$ ($p\leq0.05$ *vs*. day 7) and 5.33±1.2 $cm^3$ ($p\leq0.05$ *vs*. day 7), respectively.

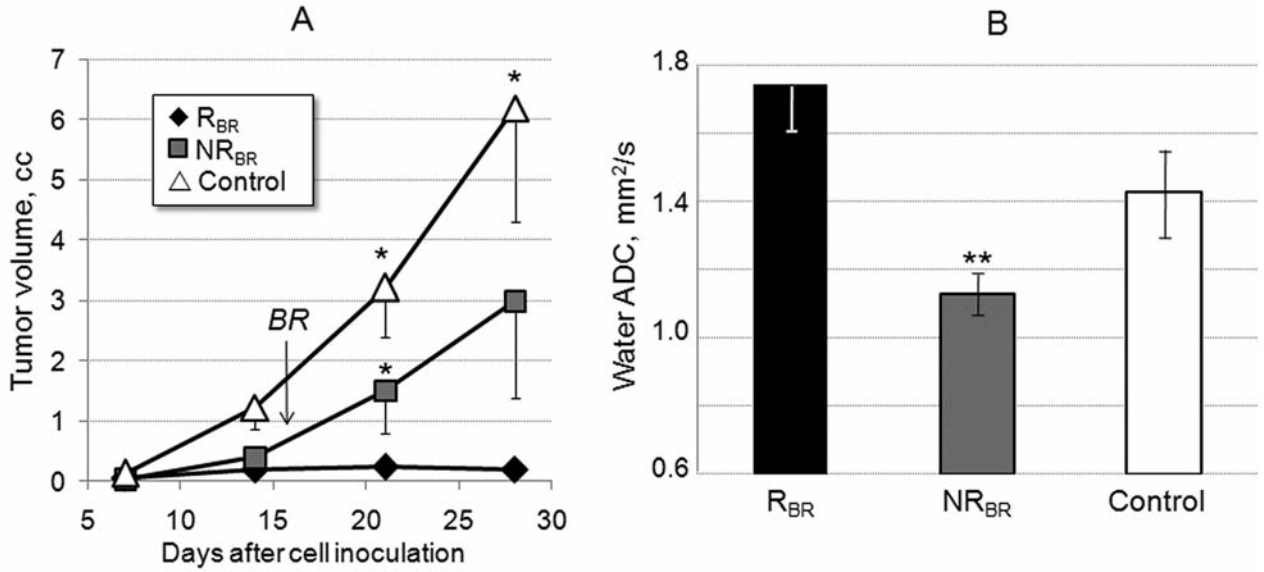


Figure 3. *Tumor volume changes (A) and water ADC 7 days before treatment (B) in $R_{BR}$ and $NR_{BR}$ HCC (M±SEM, n=12 (control), 5 ($R_{BR}$ and $NR_{BR}$)). Baseline values of water ADC were higher in $R_{BR}$ compared to $NR_{BR}$ HCCs. Significance: *p<0.05 (tumor volume: vs. day 7), **p<0.05 (ADC: $R_{BR}$ vs. $NR_{BR}$).*

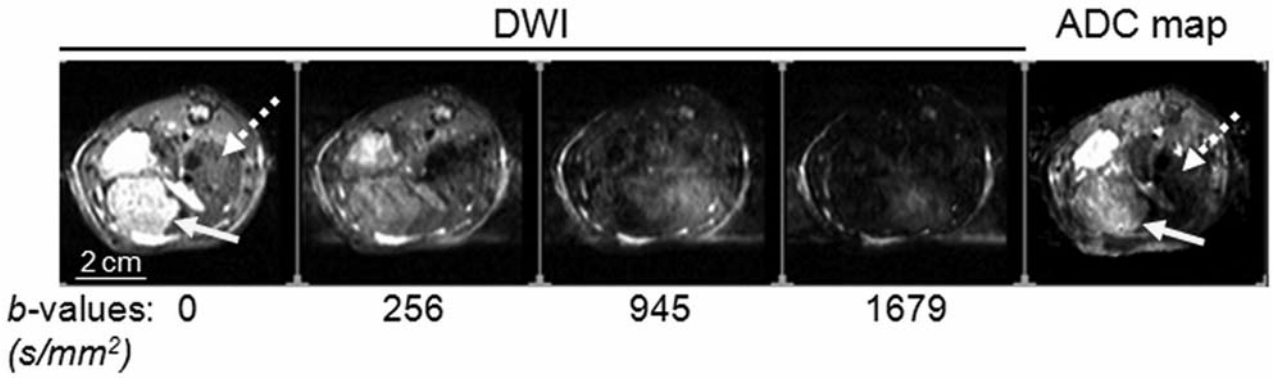


Figure 4. *DWI at different b-values and ADC map of a representative transaxial section of rat bearing HCC in the left liver lobe. HCC and surrounding normal liver are marked by solid and broken arrows, respectively.*

*Water ADC*. Figure 4 shows selected DWI transaxial sections and the ADC map of the rat liver region. HCCs (28 days after cell inoculation) are marked by solid arrows. The image of the liver containing HCC was slightly blurred with *b*-values of 945 or 1678 s/mm$^2$ even though they were collected with respiratory gating, however, the ADC map shows only a moderate motion effect in the liver area. The mean water ADC values in HCC before BR treatment (on day 7 post cell inoculation) are shown in Figure 3B and time track changes in the mean of water ADC values in HCC and nearby normal liver are shown in Figure 5. On day 7 after cell inoculation, the mean water ADC in HCC was (in $10^{-3}$mm$^2$/s) 1.23±0.08 (control group), 1.13±0.06 ($NR_{BR}$ group), and 1.74±0.14 ($R_{BR}$ group) (Figure 3B). Seven days later, the mean water ADC was not significantly changed (in $10^{-3}$ mm$^2$/s): 1.26±0.06 (control group), 1.26±0.07 ($NR_{BR}$ group), and 1.51±0.11 ($R_{BR}$ group) (Figure 5). Thus, before BR treatment, the mean water ADC was significantly ($p$<0.05) higher by 1.54 (day 7, $p$<0.05) and 1.2 times (day 14, $p$<0.05) in the $R_{BR}$ group compared to $NR_{BR}$ group.

On days 14, 21, and 28 after cell inoculation, the water ADC in control HCC remained relatively stable in the range of 1.11-1.26×10$^{-3}$ mm$^2$/s. BR treatment did not change the water ADC values in both $NR_{BR}$ and $R_{BR}$ groups. However,

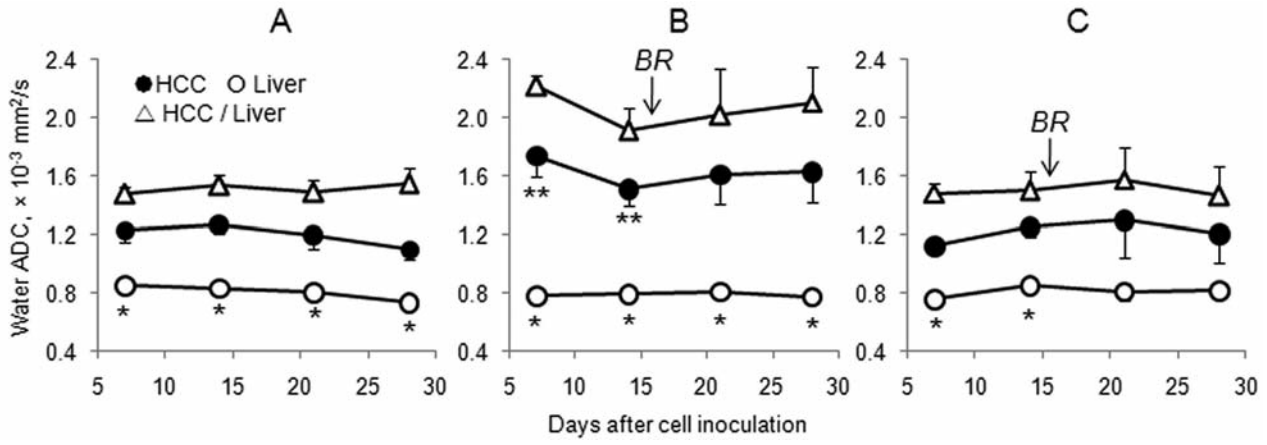


Figure 5. *Water ADC in intrahepatic HCC and surrounding normal liver tissue. A: Control, B: $R_{BR}$ tumors, C: $NR_{BR}$ tumors, (M±SEM, n=12 (control), 5 ($R_{BR}$ or $NR_{BR}$)). Water ADC in tumors was higher than in nearby liver tissue in all groups. BR did not change water ADC value in any of the groups. Significance: *p<0.05 (liver vs. HCC). **p<0.05 ($R_{BR}$ vs. $NR_{BR}$).*

the differences between these two groups were not significant after BR therapy ($p<0.15$ and $p<0.31$ on days 7 and 14 post-treatment, respectively) mostly probably due to higher variability at these data points.

In all three groups, the mean water ADC in the normal liver tissue was almost identical and unchanged during the one-month experiment. The ranges of the mean water ADC in the liver were between (in $10^{-3}$ $mm^2/s$) 0.74-0.85 (control group), 0.76-0.85 ($NR_{BR}$ group), and 0.78-0.81 ($R_{BR}$ group) (Figure 5). Before BR treatment, the mean water ADC in HCC of all three groups was significantly ($p<0.05$) higher compared to the adjacent normal liver. For example, 7 days after cell inoculation, the ratio of water ADC in the tumor to that in the liver was 1.49±0.13 (control group), 1.48±0.06 ($NR_{BR}$ group), and 2.2±0.08 ($R_{BR}$ group). After BR treatment, the mean water ADC in HCC continued to be significantly ($p<0.05$) higher compared to the adjacent normal liver in control and $R_{BR}$ groups but not in the $NR_{BR}$ group ($p<0.13$). HCC-to-liver ADC ratio did not change significantly with tumor growth in control and $NR_{BR}$ groups or with arrest of tumor growth in the $R_{BR}$ group.

## Discussion

In this work, the changes in tumor volume and water ADC in the rat HCC before and after interventional treatment of the tumor with BR were studied. The measurement of water ADC in the rat intrahepatic HCC was challenging due to respiratory, cardiac, bowel, *etc*. motions. To minimize these problems, we decreased the respiratory rate to 35–40 breaths/min and used gating to monitor water ADC only during the end-expiration time when diaphragmatic motion is reduced. In addition, the calculation of water ADC was done by: i) using thresh-holding to eliminate ADC values that were clearly higher than free water diffusion (>3 $mm^2/s$), ii) avoiding the undoubtedly bright spots on ADC maps when the region of interest was drawn, and iii) comparing water ADC in HCC and surrounding normal liver tissue, which was also undergoing similar motion effects. These approaches helped to achieve relatively steady ADC values for each experimental data point.

In HCC, the mean water ADC was significantly higher than in surrounding normal liver tissue by ~1.5 times (control and $NR_{BR}$ groups) and by ~2 times ($R_{BR}$ group) on all experimental days. BR did not change this ratio significantly. These data correlate with other publications showing higher water ADC in HCC compared to healthy liver tissue (3, 17-18). The most reasonable explanation of this effect is less differentiation of tumor cells and a net increase in the tumor relative extracellular space (ECS). Histology of HCC and liver after the last MRI experiment showed that HCC contains areas of inflammation and necrosis with increased ECS (Figure 1C) in which water ADC could be high. It has also been shown that in experimental mammary tumors, the high and low ADC values also correlate with high and low necrosis, respectively (5).

Intrahepatic infusion of BR was a semi-effective treatment of intrahepatic HCC in rats. Thus, the two groups of BR-treated animals, which differed in their sensitivity to the treatment, were identified as $R_{BR}$ and $NR_{BR}$. Tumor growth in the $R_{BR}$ group was arrested while in control and $NR_{BR}$ groups the tumor continued to grow. We have previously shown that BR induces apoptosis in rabbit and rat liver tumors with minimal apoptosis in normal liver (19-20). For example, the mean tumor apoptosis rates were 71% with 10 mg/kg BR and only 1% with saline solution treatment. BR-mediated

induction of tumor apoptosis makes BR an excellent candidate for chemotherapeutic application (12, 21).

Apoptosis and necrosis have to increase water ADC in tumor due to increase in ECS (22). However, this was not the issue in our case. After BR infusion, the water ADC remained unchanged in both $R_{BR}$ and $NR_{BR}$ groups. In our experiments, it seems that BR induced apoptotic and necrotic changes leading to increase in ECS and water ADC are counterbalanced by the ADC reducing factors. Histological analysis has shown that HCC contained coagulative type of necrosis characterized by well-packed nucleus-less cells and macromolecular contamination that can restrict water motion and thereby increase the tortuosity of this space. Monte Carlo simulation of diffusion in the ECS have shown that the extracellular volume fraction $\alpha$ and tortuosity factor $\lambda$ are interrelated by Archie's low $\lambda=\alpha^{-l}$, where $l$ is the tortuosity exponent (23). The increase of tortuosity factor has been correlated experimentally with a dynamic decrease of the ADC in ischemic brain (24). Another factor that can counterbalance a possible increase in ADC could be changes in water diffusion in intracellular space (ICS). Usually the value of ADC in ICS is underestimated beside the fact that the cells occupy 82-85% of the tissue space in the liver (25). The experimental measurements of ADC in ECS and ICS have shown that ADC values in those compartments are more identical than different (16, 26). This is in contrast to the general belief that water ADC is lower in the ICS compared to ECS.

The perfusion factor that can contribute to water ADC value could be the issue in our case (27). However, the effect of perfusion is diminished when wide ranges of *b*-values are used as it was done in this study (*b*=0, 256, 945 and 1679 s/mm$^2$). Nevertheless, this assumption needs further experimental estimation using additional *b*-values in the range 0-100 s/mm$^2$. Thoeny *et al*. (28) propose using the difference between ADCs obtained with low (0-100 s/mm$^2$) and high *b*-values (500-1000 s/mm$^2$) as a perfusion component of the tissue ADC.

It is unclear how the initial ADC values can predict tumor chemosensitivity that could be clinically relevant. Lemaire *et al*. (5) showed that 5-fluorouracil-treated experimental mammary tumors were distinguishable in terms of water ADC up to day 5 whereas the tumor volume, over the same period of time, did not distinguish the sensitive and non-sensitive groups. Contrary to these data, Seierstad *et al*. (29) did not find correlations between pretreatment ADC values and changes in colon adenocarcinoma HT29 xenograft volumes after chemoradiation, whereas early changes in mean ADC quantitatively correlated with treatment outcome. We have found that the initial levels of water ADC in the $R_{BR}$ group were higher compared to the $NR_{BR}$ group. These data suggest that a higher initial ADC level (1.5-1.7×10$^{-3}$ mm$^2$/s) could be a promising sign for effective BR treatment, and in contrast, tumors with a lower initial ADC value (1.1-1.3×10$^{-3}$ mm$^2$/s) are most likely to be resistant to BR treatment. The tumors with high initial values of water ADC were more vulnerable to BR therapy, suggesting that the cells were in weaker physiological condition. The weaker physiological condition of the cells may be related to the decreased cell membrane permeability. It has been previously shown that the more sensitive to chemotherapy with carmustine subcutaneous 9L glioma in rat had higher water ADC and $^{23}$Na signal intensity (30). Like water ADC, single quantum $^{23}$Na signal intensity mostly reflects changes in ECS. However, it was shown that ECS did not change in carmustine-treated subcutaneous 9L glioma (31). The authors found that the increase in $^{23}$Na MRI resulted from an increase in intracellular $Na^+$ following damage to the plasma membrane. Thus, $^{23}$Na MRI in conjunction with DWI could provide synergistic information of post-treatment changes in liver tumors, allowing prediction and early assessment of treatment success.

In conclusion, the data presented here show that implantation of N1S1 cells in the rat liver can be used as a HCC model for pre-clinical study of transarterial therapy with BR. Water ADC of N1S1-inoculated HCC is higher than in nearby normal liver tissue. Before BR treatment the mean water ADC is higher in the $R_{BR}$ group compared to the $NR_{BR}$ group. Intrahepatic infusion of BR is a semi-effective transarterial treatment of HCC in rats. BR therapy did not change the water ADC value regardless to tumor sensitivity. Accurate non-invasive and quantitative monitoring of the water ADC before and following chemotherapy of HCC is critical as this data may help to select an appropriate therapy or indicate a need for alteration in therapy.

## Acknowledgments

The Authors gratefully acknowledge Dr. S. Greg Jennings for valuable discussion and editorial comments. This research was supported in part by NIH grants R01CA84434, R01EB005964 and 1R33CA110107.

## References

1 Parkin DM, Bray F, Ferlay J and Pisani P: Estimating the world cancer burden: Globocan 2000. Int J Cancer *94*: 153-156, 2001.

2 Babsky A, Ju S and Bansal N: Evaluation of Tumor Treatment Response with DWI. *In*: Extra-cranial Applications of Diffusion-weighted MRI. Taouli B (ed.). Cambridge, Cambridge University Press, pp. 172-196, 2011.

3 Colagrande S, Carbone SF, Carusi LM, Cova M and Villari N: Magnetic resonance diffusion-weighted imaging: extraneurological applications. Radiol Med *111*: 392-419, 2006.

4 Padhani A, Liu G, Koh DM, Chenevert TL, Thoeny HC, Takahara T, Dzik-Jurasz A, Ross BD, Van Cauteren M, Collins D, Hammoud DA, Rustin GJ, Taouli B and Choyke PL: Diffusion-weighted magnetic resonance imaging as a cancer biomarker: consensus and recommendations. Neoplasia *11*: 102-125, 2009.

5 Lemaire L, Howe FA, Rodrigues LM and Griffiths JR: Assessment of induced rat mammary tumour response to chemotherapy using the apparent diffusion coefficient of tissue water as determined by diffusion-weighted $^{1}$H-NMR spectroscopy *in vivo*. MAGMA *8*: 20-26, 1999.
6 Morse DL, Galons JP, Payne CM, Jennings DL, Day S, Xia G and Gillies RJ: MRI-measured water mobility increases in response to chemotherapy *via* multiple cell-death mechanisms. NMR Biomed *20*: 602-614, 2007.
7 Thoeny HC, De Keyzer F, Chen F, Vandecaveye V, Verbeken EK, Ahmed B, Sun X, Ni Y, Bosmans H, Hermans R, van Oosterom A, Marchal G and Landuyt W: Diffusion-weighted magnetic resonance imaging allows noninvasive *in vivo* monitoring of the effects of combretastatin a-4 phosphate after repeated administration. Neoplasia *7*: 779-787, 2005.
8 Taouli B and Koh DM: Diffusion-weighted MRI of the liver. *In*: Extra-cranial Applications of Diffusion-weighted MRI. Taouli B (ed.). Cambridge, Cambridge University Press, pp. 18-31, 2011.
9 Kim T, Murakami T, Takahashi S, Hori M, Tsuda K and Nakamura H: Diffusion-weighted single-shot echoplanar MR imaging for liver disease. AJR Am J Roentgenol *173*: 393-398, 1999.
10 Chen CY, Li CW, Kuo YT, Jaw TS, Wu DK, Jao JC, Hsu JS and Liu GC: Early response of hepatocellular carcinoma to transcatheter arterial chemoembolization: choline levels and MR diffusion constants – initial experience. Radiology *239*: 448-456, 2006.
11 Guan S, Zhou K, Zhao W, Peng W, Tang F and Mao J: Magnetic resonance diffusion-weighted imaging in the diagnosis of diffuse liver diseases in rats. Chin Med J (Engl) *118*: 639-644, 2005.
12 Salamon A, Hagenauer B, Thalhammer T, Szekeres T, Krohn K, Jayaram HN and Jager W: Metabolism and disposition of the novel antileukaemic drug, benzamide riboside, in the isolated perfused rat liver. Life Sci *69*: 2489-2502, 2001.
13 Hayashi M, Matsui O, Ueda K, Kawamori Y, Gabata T and Kadoya M: Progression to hypervascular hepatocellular carcinoma: correlation with intranodular blood supply evaluated with CT during intraarterial injection of contrast material. Radiology *225*: 143-149, 2002.
14 Ju S, McLennan G, Bennett SL, Liang Y, Bonnac L, Pankiewicz KW and Jayaram HN: Technical aspects of imaging and transfemoral arterial treatment of N1-S1 tumors in rats: an appropriate model to test the biology and therapeutic response to transarterial treatments of liver cancers. J Vasc Interv Radiol *20*: 410-414, 2009.
15 Sigmund EE and Jensen J: Basic physical principles of body diffusion-weighted MRI. *In*: Extra-cranial Applications of Diffusion-weighted MRI. Taouli B (ed.). Cambridge, Cambridge University Press, pp. 1-17, 2011.
16 Duong TQ, Ackerman JJ, Ying HS and Neil JJ: Evaluation of extra- and intracellular apparent diffusion in normal and globally ischemic rat brain *via* $^{19}$F NMR. Magn Reson Med *40*: 1-13, 1998.
17 Sun X, Wang H, Chen F, De Keyzer F, Yu J, Jiang Y, Feng Y, Li J, Marchal G and Ni Y: Diffusion-weighted MRI of hepatic tumor in rats: Comparison between *in vivo* and postmortem imaging acquisitions. J Magn Reson Imaging *29*: 621-628, 2009.
18 Yamada I, Aung W, Himeno Y, Nakagawa T and Shibuya H: Diffusion coefficients in abdominal organs and hepatic lesions: evaluation with intravoxel incoherent motion echo-planar MR imaging. Radiology *210*: 617-623, 1999.
19 McLennan G, Bennett SL, Ju S, Babsky A, Bansal N, Shorten ML, Bonnac L, Panciewicz KW and Jayaram HN: Tumor response and apoptosis of N1-S1 rodent hepatomas in response to intra-arterial and intravenous benzamide riboside. Cardiovasc Intervent Radiol DOI 10.007/s00270-011-0140-z, Mar 24, 2011.
20 McLennan G, Cressman EN, Xu Y, Zhang D, Jagtap MR and Jayaram HN: The effect of benzamide riboside on the VX2 model of liver cancer in rabbits. J Vasc Interv Radiol *16*: 1499-1504, 2005.
21 Jager W, Salamon A and Szekeres T: Metabolism of the novel IMP dehydrogenase inhibitor benzamide riboside. Curr Med Chem *9*: 781-786, 2002.
22 Koh DM and Collins DJ: Diffusion-weighted MRI in the body: applications and challenges in oncology. AJR Am J Roentgenol *188*: 1622-1635, 2007.
23 Lipinski H: Monte Carlo simulation of extracellular diffusion in brain tissues. Phys Med Biol *35*: 441-447, 1990.
24 Pfeuffer J, Dreher W, Sykova E and Leibfritz D: Water signal attenuation in diffusion-weighted $^{1}$H NMR experiments during cerebral ischemia: influence of intracellular restrictions, extracellular tortuosity, and exchange. Magn Reson Imaging *16*: 1023-1032, 1998.
25 Makos JD, Malloy CR and Sherry AD: Distribution of $TmDOTP^{5-}$ in rat tissues: $TmDOTP^{5-}$ *vs*. CoEDTA as markers of extracellular tissue space. J Appl Physiol *85*: 1800-1805, 1998.
26 Babsky AM, Topper S, Zhang H, Gao Y, James JR, Hekmatyar SK and Bansal N: Evaluation of extra- and intracellular apparent diffusion coefficient of sodium in rat skeletal muscle: effects of prolonged ischemia. Magn Reson Med *59*: 485-491, 2008.
27 Le Bihan D, Breton E, Lallemand D, Aubin ML, Vignaud J and Laval-Jeantet M. Separation of diffusion and perfusion in intravoxel incoherent motion MR imaging. Radiology *168*: 497-505, 1988.
28 Thoeny HC, De Keyzer F, Chen F, Ni Y, Landuyt W, Verbeken EK, Bosmans H, Marchal G and Hermans R: Diffusion-weighted MR imaging in monitoring the effect of a vascular targeting agent on rhabdomyosarcoma in rats. Radiology *234*: 756-764, 2005.
29 Seierstad T, Folkvord S, Roe K, Flatmark K, Skretting A and Olsen DR: Early changes in apparent diffusion coefficient predict the quantitative antitumoral activity of capecitabine, oxaliplatin, and irradiation in HT29 xenografts in athymic nude mice. Neoplasia *9*: 392-400, 2007.
30 Babsky A, Hekmatyar S, Zhang H, Solomon J and Bansal N: Predicting and monitoring response to chemotherapy by 1,3-*bis*(2-chloroethyl)-1-nitrosourea in subcutaneously implanted 9L glioma using the apparent diffusion coefficient of water and $^{23}$Na MRI. J Magn Reson Imaging *24*: 132-139, 2006.
31 Winter PM, Poptani H and Bansal N: Effects of chemotherapy by 1,3-*bis*(2-chloroethyl)-1-nitrosourea on single-quantum- and triple-quantum-filtered $^{23}$Na and $^{31}$P nuclear magnetic resonance of the subcutaneously implanted 9L glioma. Cancer Res *61*: 2002-2007, 2001.

*Received April 27, 2011*
*Revised May 18, 2011*
*Accepted May 19, 2011*